Hindawi
Mathematical Problems in Engineering
Volume 2022, Article ID 2213697, 11 pages
https://doi.org/10.1155/2022/2213697

Research Article

LQR Active Control of Fractional-Order Pantograph-Catenary System Based on Feedback Linearization

Beining Wang[1,2], **Shaofang Wen**[2,3] **and Yongjun Shen**[3]

[1]*Key Laboratory of Traffic Safety and Control of Hebei Province, Shijiazhuang 050043, China*
[2]*School of Traffic and Transportation, Shijiazhuang Tiedao University, Shijiazhuang 050043, China*
[3]*State Key Laboratory of Mechanical Behavior and System Safety of Traffic Engineering Structures, Shijiazhuang Tiedao University, Shijiazhuang 050043, China*

Correspondence should be addressed to Shaofang Wen; wsf39811@163.com

Received 21 March 2022; Accepted 14 October 2022; Published 21 October 2022

Academic Editor: Haijun Ren

Fractional-order calculus has exclusive advantages in modeling the viscoelastic components with obvious fractional-order characteristics such as air springs and metal rubbers in the pantograph structure. In this paper, the air spring is tested, and fractional-order calculus is applied to the modeling of pantograph-catenary system of the high-speed train. The parameter identification method of fractional-order derivative is analytically derived. The traditional lumped mass model is improved and a coupling two-degree-of-freedom model of the fractional-order pantograph-catenary system is established. The fractional-order derivative term in the pantograph-catenary model is approximately calculated by the Oustaloup filter algorithm. Taking the time-varying nature into consideration, the catenary is treated as an extended variable to obtain an augmented model. On this basis, the system is linearized based on differential geometry theory, and an LQR controller is designed to control the pantograph-catenary system. The feedback linearized LQR control and PID control are used to control the same type of traditional pantograph, and the results are compared. Meanwhile, the control effects of feedback linearized LQR control under different pantograph parameters and at different train speeds are analyzed. The results show that the feedback linearized LQR control can present a much better control performance than PID control, and the pantograph-catenary contact force and pantograph head vibration amplitude are both reduced obviously. Even at different train speeds or under different pantograph parameters, it can also effectively reduce these control indexes and provide more robust control performance. These results help to put forward new control ideas and theoretical basis for the vibration control of the pantograph-catenary or similar dynamical system.

1. Introduction

With the constant improvement of train speeds, the fluctuation of the contact force between the pantograph and catenary increases, which will result in unstable current receiving quality. Therefore, higher requirements are put forward for the current receiving performance of high-speed trains. As the direct power supply equipment for electrified railway, the power supply performance of the pantograph-catenary system directly affects the safety and stability of the railway operation. Due to the nonlinear and nonsmooth characteristics of the pantograph structure, the vibration of the train body, and the special excitation of the catenary, the actual working conditions of the pantograph at the high speed are very complicated. How to accurately describe the dynamic behavior of the pantograph-catenary system of the high-speed train, how to effectively control it, and how to improve the current receiving quality and ensure the safe operation of the high-speed train have become a hot research topic.

Since the 1950s, many studies on the dynamics of pantograph, catenary, and pantograph-catenary interaction have been carried out. A series of theoretical models of pantograph-catenary system have been established gradually, of which the pantograph model and catenary model were continuously improved and expanded [1–5]. Lee et al. [1] established a three-dimensional catenary model considering factors such as slackening of the dropper, pre-sag, and stagger, and the reliability of the model was verified. Massat et al. [2]

coupled the finite element catenary model with the full flexible multibody pantograph model for co-simulation, which improved the simulation efficiency. Hu et al. [3] studied the transient dynamic response of the whole dropper under the interaction of pantograph and catenary based on the simple chain-shaped suspension catenary. Zhang et al. [4] established the models of train, line, and pantograph-catenary, respectively, and then coupled them into a unified system. The pantograph models mainly include lumped mass model, multirigid body model, rigid-flexible hybrid model, and fully flexible model [6]. However, most of the lumped mass models are integer-order ones, and the influences of nonlinear devices such as air springs in the pantograph structure are not considered enough. Vibration damping devices such as air springs, metal rubbers, and intelligent dampers all have memory characteristics. It is difficult for the traditional integer-order models to accurately describe these material characteristics. In contrast, fractional-order models can better reflect the memory characteristics of materials. Since the emergence of fractional calculus theory, scholars have carried out extensive research on it [7–12]. Lopes et al. [7] showed that fractional-order models could describe the memory characteristics of materials more accurately than integer-order models in electric engineering. Liu et al. [8] established a fractional-order Bingham model for magneto-rheological fluid damper, and the experimental results showed that the fitting accuracy of the fractional-order Bingham model was significantly higher than that of the traditional Bingham model. Zhang et al. [9] proved that the fractional-order Maxwell model could effectively describe the whole creep process of asphalt mixture under different stress levels through experiments. Peng et al. [10] applied fractional calculus to the wellbore creep model. By comparing with the classical model, it was found that the fitting accuracy of the fractional-order model was higher for viscoelastic materials. Obviously, in the pantograph-catenary system with viscoelastic devices, the fractional-order model may achieve higher fitting accuracy with fewer parameters.

In the research on vibration control of pantograph-catenary system, in addition to improving the dynamic characteristics of pantograph-catenary system by optimizing the performance parameters of pantograph and catenary structure, active control based on modern control theory is also applied to suppress the fluctuation of the contact force, and the current receiving quality of pantograph-catenary system will be improved. Optimal control [13–19], variable structure control [20–23], and fuzzy control [24–28] are commonly used in vibration control of pantograph-catenary system. LQR optimal control takes the minimum system performance index as the evaluation function [19], which can achieve the optimal control effect with small control energy. Guo et al. [13] applied the LQR control to the two-degree-of-freedom linear pantograph-catenary model, obtained the optimal control law by solving the Riccati equation, and compared the control effect of the active control force acting on different positions. Due to the time-varying stiffness of the catenary, there are limitations in directly applying the control strategy of the linear system to the pantograph-catenary system. If the algebraic Riccati equation is used to solve the problem, the influence of the time-varying stiffness of the catenary is not fully considered and then the calculation accuracy decreased. From the perspective of controlling the tracking error, Chen et al. [14] used the LQR control algorithm to design the output tracker to adapt to the time-varying stiffness of catenary and improve the calculation accuracy. For the time-varying stiffness of catenary, the linear pantograph-catenary model is transformed into a nonlinear model [15, 17–19], and the controller based on feedback linearization is designed. Ren et al. [29] designed a feedforward controller for wind turbine based on feedback linearization with sliding mode and fuzzy PID algorithm. Liu et al. [30] applies the feedback linearization method to the state observation of a nonlinear quarter car model with an air spring. Xia [31] designed controllers for two kinds of fractional-order T-S fuzzy systems based on state feedback and achieved good control effects. Accordingly, it is necessary and feasible to establish the fractional-order pantograph-catenary system model with an air spring and apply the feedback linear method to design its controller.

In this paper, the viscoelastic characteristic of air springs is studied experimentally. The fractional-order model of the air spring is established by using fractional calculus theory, and then the traditional two-degree-of-freedom pantograph-catenary model is improved. Compared with the traditional integer-order pantograph-catenary model, a more accurate fractional-order pantograph-catenary model is established. The time-varying stiffness of catenary is treated as the extended state variable to obtain the augmented model. The inner and outer state equations of the augmented model are derived by using the theory of differential homeomorphic transformation. On this basis, the LQR controller is designed to actively control the pantograph-catenary system. Through numerical simulation, the effect of the LQR control designed on the vibration control of the pantograph-catenary system is analyzed under different pantograph parameters and at different speeds. At the same time, the PID controller is designed. The control effects and performance indicators of the two active controllers are compared and analyzed when the active control forces act on the frame.

2. Modeling of Fractional-Order Pantograph-Catenary System

2.1. Fractional-Order Modeling of Air Springs. The primary experimental equipment is the HT-9711 material fatigue testing machine produced by Taiwan Hongda Group Co., Ltd. The test equipment and the ContiTech air spring used are shown in Figure 1.

With different pressures, amplitudes, and frequencies for experiments, it is found that the viscoelastic characteristics of the air spring under dynamic load are more obvious. In order to correct the difference between the model and the experimental results, the fractional-order theory is introduced [32]. The fractional-order model of the air spring is established as

$$F_a(t) = K\left[D_t^{\alpha} x(t)\right], \tag{1}$$

where F_a represents the force of the air spring. K is the fractional-order differential coefficient, $x(t)$ denotes the

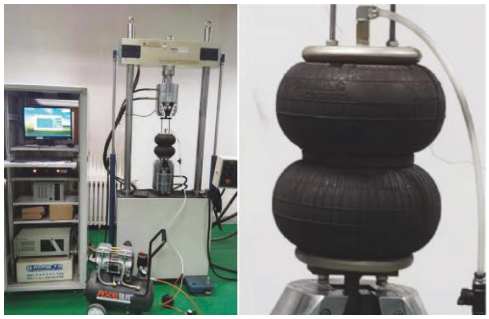

Figure 1: Air springs and experimental equipment.

displacement, and $D_t^\alpha x(t)$ represents the α -order derivative of x with respect to t $(0< \alpha <1)$.

The forced excitation loaded in the experiment is a sinusoidal excitation, which is

$$x(t) = z\sin(\omega t + \varphi), \tag{2}$$

where z is the excitation amplitude, ω is the angular velocity, and φ is the phase.

We substitute (2) into (1), and through Laplace transform, it can be obtained

$$L[F_a(t)] = KL[D_t^\alpha x(t)] = Kz\left[\omega\cos\varphi\frac{S^\alpha}{S^2+\omega^2} + \sin\varphi\frac{S^{\alpha+1}}{S^2+\omega^2}\right]. \tag{3}$$

According to the inverse Laplace transform,equation (3) becomes

$$F_a(t) = Kz\left\{\omega\cos\beta L^{-1}[\nabla_1] + \sin\beta L^{-1}[\nabla_2]\right\}, \tag{4}$$

where $\nabla_1 = S^\alpha/S^2+\omega^2$, $\nabla_2 = S^{\alpha+1}/S^2+\omega^2$. The singularity of ∇_1 is $S = \pm i\omega$. According to the residue theorem, the inverse Laplace transform of ∇_1 is

$$L^{-1}[\nabla_1] = \frac{(\mathrm{i}\omega)^\alpha}{\mathrm{i}2\omega}\mathrm{e}^{\mathrm{i}\omega t} + \frac{(-\mathrm{i}\omega)^\alpha}{-\mathrm{i}2\omega}\mathrm{e}^{-\mathrm{i}\omega t}. \tag{5}$$

We use the equation

$$\mathrm{i}^\alpha = \left(\mathrm{e}^{\mathrm{i}\pi/2}\right)^\alpha = \mathrm{e}^{\mathrm{i}\alpha\pi/2}. \tag{6}$$

We substitute equation (6) into (5), and simplify it

$$L^{-1}[\nabla_1] = \frac{\omega^\alpha}{\omega}\sin(\alpha\pi/2 + \omega t). \tag{7}$$

According to the same process, it can be obtained

$$L^{-1}[\nabla_2] = \omega^\alpha\sin(\alpha\pi/2 + \pi/2 + \omega t). \tag{8}$$

We substitute (7) and (8) into (4), and simplify it

$$F_a(t) = Kz\omega^\alpha\sin(\alpha\pi/2 + \omega t + \varphi). \tag{9}$$

Selecting the experimental parameters as the pressure $P = 0.1$ MPa, the excitation amplitude $z = 6$ mm, and the frequency as 1 Hz, the measured results of the displacement and force are shown in Figure 2, represented by " $*$ ". The fractional-order α and coefficient K of (1) are obtained by the least square method. The force-displacement fitting curve is also shown in Figure 2, represented by the solid red line. Through the data simulation and comparison, it is found that the data simulated by the fractional-order model agrees well with the experimental data. It shows that the fractional-order model proposed in this paper can well reflect the viscoelastic characteristics of the air spring.

2.2. Pantograph-Catenary Model. To study the complex dynamics of pantograph-catenary system conveniently, the pantograph and catenary are simplified into mathematical models separately at first. Then, the pantograph model and catenary model are coupled to obtain the dynamic model of the pantograph-catenary system.

The stiffness of the catenary varies continuously within and between spans due to the different contact locations. In the simplified analysis, the catenary is regarded as a variable stiffness elastic system. In ref. [13], Guo et al. used the least squares method to fit the actual stiffness curve calculated by the finite element method and obtained the simplified catenary stiffness formula. It can be described as

$$k(t) = k_0\left(1 + \alpha_1 f_1 + \alpha_2 f_2 + \alpha_3 f_1^2 + \alpha_4 f_3^2 + \alpha_5 f_4^2\right). \tag{10}$$

Among them, $f_1 = \cos(2\pi vt/L)$, $f_2 = \cos(2\pi vt/L_1)$, $f_3 = \cos(\pi vt/L)$, $f_4 = \cos(\pi vt/L_1)$, where v represents the train speed, m/s. L represents the catenary span, m. L_1 represents the distance between the adjacent hanging strings of the catenary, m. k_0 represents average stiffness, N/m. $\alpha_i\,(i = 1, 2, 3, 4, 5)$ represents stiffness difference coefficient.

In this study, the simple chain suspension is used [13, 19]. For simple chain suspension catenary, there are $k_0 = 3684.5$, $\alpha_1 = 0.4665$, $\alpha_2 = 0.0832$, $\alpha_3 = 0.2603$, $\alpha_4 = -0.2801$, $\alpha_5 = -0.3364$.

In the research of the vibration control of pantograph-catenary system, the pantograph is usually simplified to a lumped mass model composed of linear stiffness and linear damping, as is shown in Figure 3. In this paper, a two-degree-of-freedom pantograph model is chosen as the basis. Take into consideration of the viscoelastic properties of vibration damping devices in pantograph-catenary systems, it is difficult to use the integer-order model to describe its performance well with fewer parameters. Therefore, the fractional-order model of the air spring is introduced into the model of the pantograph-catenary system, as is shown in Figure 4.

The system dynamical equation is

$$\begin{cases} m_1\ddot{z}_1 + k_1(z_1 - z_2) + c_1(\dot{z}_1 - \dot{z}_2) + k(t)z_1 = 0, \\ m_2\ddot{z}_2 + k_1(z_2 - z_1) + c_1(\dot{z}_2 - \dot{z}_1) + c_2(\dot{z}_2 - \dot{z}_r) + kD_t^p(z_2 - z_r) = F, \end{cases} \tag{11}$$

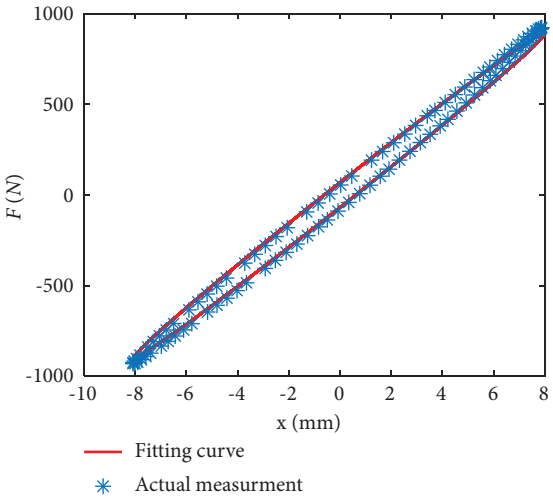

Figure 2: Comparison of experimental and fitting curves.

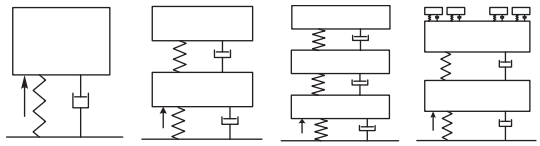

Figure 3: Lumped mass model of pantograph.

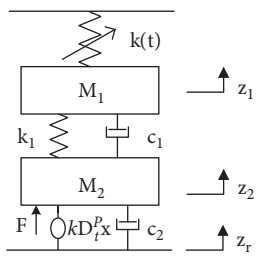

Figure 4: Two-degree-of-freedom model of pantograph-catenary.

where m_1, m_2 are the mass of the collector and frames of a pantograph, respectively. k_1 represents the stiffness of the collector. k represents the fractional differential term coefficient. c_1, c_2 represent the damping of the collector and frame, respectively. z_1, z_2 denote the vertical displacement of each mass. z_r is the locomotive body excitation. $k(t)$ represents catenary stiffness. F is the active control force, which consists of the control force $u(t)$ and the static lifting force f_0.

2.3. Oustaloup Filter Approximation Algorithm for Fractional Calculus. At present, there are three main forms of definitions for fractional calculus [12], i.e., Riemann–Liouville definition, Grunwald–Letnikov definition, and Caputo definition. In this paper, the Caputo definition is used as

$$D_t^p x(t) = \frac{1}{\Gamma(1-p)} \int_0^t \frac{\dot{x}(\tau)}{(t-\tau)^p} d\tau, \tag{12}$$

where $\Gamma(y)$ is the Gamma function and p is the fractional order.

For simulation, the Oustaloup filter algorithm [12] is used in the approximate calculation of fractional calculus. In the selected frequency band (ω_b, ω_h), the approximate substitution of fractional operators s^p is obtained and the Oustaloup filter is constructed as

$$s^p \approx \omega_h^p \prod_{i=1}^{M} \frac{s+\omega_i^*}{s+\omega_i}, \tag{13}$$

where M is the order of the filter, the zero point of the filter is $\omega_i^* = \omega_b (\sqrt{\omega_h/\omega_b})^{(2i-1-p)/M}$, and the pole point is $\omega_i = \omega_b (\sqrt{\omega_h/\omega_b})^{(2i-1-p)/M}$.

When the fractional operator is $s^{0.5}$, M is selected as 5, 7, and 9, respectively, and the results are shown in Figure 5. In the frequency range (0.001 rad/s, 1000 rad/s), the higher the value of filter order M, the higher the approximate accuracy of Oustaloup filter algorithm. Considering the computation accuracy and complexity, the filter order M is selected as 9.

3. LQR Active Control Based on Feedback Linearization

3.1. State Space Representation of Fractional Pantograph-Catenary System. In order to analyze the control strategy, the following state variables are defined as follows:

$$X = [x_1, x_2, x_3, x_4]^{\mathrm{T}} = [z_1, \dot{z}_1, z_2, \dot{z}_2]^{\mathrm{T}}. \tag{14}$$

The input variable is the active control force:

$$F = u(t) + f_0, \tag{15}$$

where $u(t)$ is the control force and f_0 is the static lifting force.

Let $w = \dot{z}_r$, the state space equation and output equation of (11) are

$$\begin{bmatrix} \dot{X} = f(x) + g(x)F + Dw, \\ Y = h(x), \end{bmatrix}, \tag{16}$$

3.2. Augmented Model of Fractional-Order Pantograph-Catenary System. The time-varying stiffness $k(t)$ of the catenary is treated as an extended variable to obtain an augmented model. Let $\overline{k}(t) = k(t) - k_0$, and the extended state variables are $x_5 = \overline{k}(t)$, $x_6 = \overline{k}(t)$, $\dot{x}_6 = \dot{\overline{k}}(t)$. Then, the expanded state variables are

$$X = [x_1, x_2, x_3, x_4, x_5, x_6]^{\mathrm{T}} = \left[z_1, \dot{z}_1, z_2, \dot{z}_2, \overline{k}(t), \dot{\overline{k}}(t)\right]^{\mathrm{T}}. \tag{17}$$

The augmented nonlinear affine model is

$$\begin{bmatrix} \dot{X} = f(x) + g(x)F + Dw, \\ Y = h(x), \end{bmatrix}. \tag{18}$$

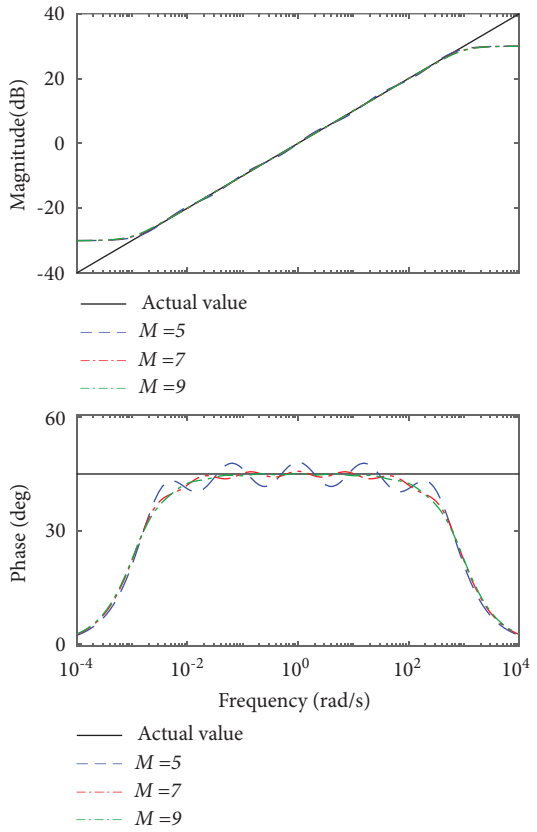

Figure 5: Bode fitting curve of oustaloup filter.

3.3. Feedback Linearization of Fractional Pantograph-Catenary System. For an n -order nonlinear system with r-order relative order, where $r \le n$, the system can be transformed into the form of internal and external state equations through differential homeomorphic transformation, so that the controller can be designed [33, 34].

According to Lie derivative, when $k = 0$, there is

$$L_g L_f^0 h(x) = \frac{\partial L_f^0 h(x)}{\partial X^{\mathrm{T}}} g(x) = \frac{\partial h(x)}{\partial X^{\mathrm{T}}} g(x) = 0, \tag{19}$$

when $k = 1$, there is

$$L_g L_f^1 h(x) = \frac{L_f^1 h(x)}{\partial X^{\mathrm{T}}} g(x) = \frac{\partial \left[\left(\partial L_f^0 h(x) / \partial X^{\mathrm{T}} \right) f(x) \right]}{\partial X^{\mathrm{T}}} g(x) = 0, \tag{20}$$

when $k = 2$, there is

$$L_g L_f^2 h(x) = \frac{\partial \left[L_f^2 h_1(x) \right]}{\partial X^T} g(x) = \frac{c_1 (x_5 + k_0)}{m_1 m_2} \neq 0. \tag{21}$$

From this, it can be found that the relative order of the system is $r = 3$, and the dimension of the system is $n = 6$, There is $r \le n$, so the system can be linearized by using homeomorphic differentiation [34].

A differential homeomorphic transformation is performed on the system, and the transformed state is w, which consists of the external state ξ and the internal state η . It is

$$w = W(x) = \left[\xi^{\mathrm{T}} \ \ \eta^{\mathrm{T}} \right]^{\mathrm{T}}, \tag{22}$$

where $\xi^T = \left[w_1 \ \ w_2 \ \ w_3 \right] = \left[h(x) \ \ L_f h(x) \ \ L_f^2 h(x) \right]$, $\eta^T = \left[w_4 \ \ w_5 \ \ w_6 \right] = \left[x_4 \ \ x_5 \ \ x_6 \right]$, $w_1 = h(x) = k_0 x_1 + x_5 x_1$, $w_2 = L_f h(x) = x_2 (k_0 + x_5) + x_1 x_6$, $w_3 = L_f^2 h(x) = 2x_2 x_6 - (k_0 + x_5/m_1)(k_1 (x_1 - x_3) + c_1 (x_2 - x_4) + k_0 x_1 + x_5 x_1) + x_1 \dot{x}_6$.

Take a derivative of w, and we can get its Jacobi matrix

$$\frac{\partial w}{\partial x^{\mathrm{T}}} = \begin{bmatrix} k_0 + x_5 & 0 & 0 & 0 & x_1 & 0 \\ x_6 & k_0 + x_5 & 0 & 0 & x_2 & x_1 \\ ① & 2x_6 - \dfrac{(k_0 + x_5)c_1}{m_1} & \dfrac{(k_0 + x_5)k_1}{m_1} & \dfrac{(k_0 + x_5)c_1}{m_1} & ② & 2x_2 \\ 0 & 0 & 0 & 1 & 0 & 0 \\ 0 & 0 & 0 & 0 & 1 & 0 \\ 0 & 0 & 0 & 0 & 0 & 1 \end{bmatrix}, \tag{23}$$

where ① $= \dot{x}_6 - ((k_0 + x_5)/m_1)(k_1 + k_0 + x_5)$, ② $= -1/m_1 (k_1 (x_1 - x_3) + c_1 (x_2 - x_4) + 2k_0 x_1 + 2x_5 x_1)$.

It can be seen that this matrix is nonsingular, so it can be proved that the transformation w is a homeomorphic differential transformation that satisfies the requirements. After the transformation, the following state feedback control law is imposed on the system

$$u(t) = \left[L_g L_f^2 h(x) \right]^{-1} \left[-L_f^3 h(x) + v \right]. \tag{24}$$

After differential homeomorphism transformation, the dynamic equation of the system is obtained, which is composed of the internal state equation, the external state equation, and the output equation as

$$\begin{cases} \dot{\eta} = q(w) + p(w)u, \\ \dot{\xi} = A_c \xi + B_c v, \\ y = C_c \xi, \end{cases} \tag{25}$$

where $q(w) = \left[j_2(x) \ \ w_6 \ \ \dot{w}_6 \right]^{\mathrm{T}}$, $p(w) = \left[1/m_2 \ \ 0 \ \ 0 \right]^{\mathrm{T}}$, $A_c = \begin{bmatrix} 1 & 0 & 0 \\ 0 & 1 & 0 \\ 0 & 0 & 1 \end{bmatrix}$, $B_c = \left[0 \ \ 0 \ \ 1 \right]^{\mathrm{T}}$, $C_c = \left[1 \ \ 0 \ \ 0 \right]^{\mathrm{T}}$.

3.4. Design of LQR Controller. In order to improve the working performance of pantograph, reduce the fluctuation of contact force, and improve the receiving quality, the vibration amplitude of pantograph head should be reduced as much as possible. The linear quadratic optimal control strategy is adopted to design the controller in the external state equation. The performance index function of the controller is determined as

$$J = \lim_{T \longrightarrow \infty} \int_0^T \left(X^{\mathrm{T}} Q X + v^{\mathrm{T}} R v \right) dt, \tag{26}$$

where R is the control energy weighting coefficient, and Q is the state weight matrix. Here, $R = 10^{-7}$ and $Q = \mathrm{diag}[\,1000\ \ 0\ \ 0\,]$.

The optimal control law that satisfies (26) is

$$\begin{cases} v = -KX, \\ K = R^{-1}B^{\mathrm{T}}P^{\mathrm{T}}, \end{cases} \tag{27}$$

where $K = [\,K_1\ \ K_2\ \ K_3\,]$ is the solution of the Riccati equation

$$A^{\mathrm{T}}P + PA - PBR^{-1}B^{\mathrm{T}}P + Q = 0. \tag{28}$$

Solving the Riccati equation and we can get $K = [\,100000\ \ 4310\ \ 90\,]$. Therefore, the optimal control force of LQR is

$$v = 10^5 w_1 + 4310 w_2 + 90 w_3. \tag{29}$$

Substitute (29) into (24), and the LQR optimal control force of the fractional-order pantograph-catenary system based on feedback linearization can be obtained

$$u(t) = \left[L_g L_f^2 h(x)\right]^{-1}\left[10^5 w_1 + 4310 w_2 + 90 w_3 - L_f^3 h(x)\right]. \tag{30}$$

4. Simulation Study

The pantograph will be affected by external excitation from the locomotive body in train operation. In this paper, the locomotive body excitation is approximated as a Gaussian white noise signal. The passive control simulation model, PID control simulation model, and feedback linearized LQR active control simulation model are established in Simulink, respectively. The following simulation results are all in a steady state, and the blue line represents passive control, the red line represents the feedback linearized LQR active control, and the green line represents PID control.

4.1. Simulation of Different Pantograph Parameters. In order to prove that the LQR active control method in this paper can be applied to different types of pantographs, two types of traditional pantograph parameters [16, 23] are selected, and the specific parameters are shown in Table 1.

When train speed is 250 km/h, the simulation results of Type I pantograph under passive control and active control are shown in Figure 6, and the simulation results of Type II pantograph are shown in Figure 7. The comparison of pantograph-catenary contact force and pantograph head displacement in the steady state are shown in Tables 2 and 3, respectively. It can be seen that feedback linearized LQR active control can achieve good control effects for the two types of pantographs, and the active control force fluctuates are controlled within the range of (70–100) N and (50–90) N, respectively. It can be seen from Table 2 that for Type I pantograph, the feedback linearization LQR control reduces the mean and the standard deviation of the contact force by 14% and 23% respectively, and the mean and the standard deviation of pantograph head displacement are reduced by 17% and 31%, respectively. It can be seen from Table 3 that for Type II pantograph, the feedback linearization LQR control reduces respectively the mean and the standard deviation of the contact force 26% and 49%, respectively, and the mean and the standard deviation of pantograph head displacement are reduced by 28% and 50%, respectively. It can be concluded that the feedback linearized LQR active control can effectively reduce the pantograph-catenary contact force and the vibration amplitude of the pantograph head, and make more stable for different types of pantographs.

4.2. Compared with PID Control Simulation. In order to verify the control effect of feedback linearization LQR active control, PID active control and feedback linearization LQR active control are used for simulation and comparison.

We take the performance index of the pantograph-catenary contact force as the control quantity, and a PID controller is designed to control the pantograph-catenary system. The expected value of the pantograph-catenary contact force is set to 100 N, and the parameter optimization objective function of the PID controller is constructed as follows:

$$J = \lim_{T\longrightarrow\infty}\int_0^T F^2 dt, \tag{31}$$

where F is the actual pantograph-catenary contact force.

The input signal of the PID controller is

$$e(t) = F_N - F, \tag{32}$$

where F_N is the expected value of pantograph-catenary contact force, and F is same as above.

The output signal of the PID controller is the active control input force by the nonlinear fractional-order pantograph-catenary system

$$u(t) = K_p e(t) + K_I\int e(t)dt + K_D\frac{de(t)}{dt}, \tag{33}$$

where K_p, K_I, K_D are the proportional, integral, and differential coefficients of the PID active controller, respectively.

For Type I pantograph, when train speed is 250 km/h, the response curve of the pantograph-catenary system is continuously analyzed through the trial and error method, and the optimal PID control parameters that meet the control requirements are selected after multiple comparisons. There are $K_p = 4.5$, $K_I = 0.5$, and $K_D = 0.01$. The two control methods are simulated with Type I pantograph. When train speed is 250 km/h, the comparison of the results of the two control methods is shown in Figure 8, and the statistical comparison of the performance indicators is shown in Table 4.

From Figure 8 and Table 4, it can be seen that when train speed is 250 km/h, both PID control and feedback linearized LQR control can effectively improve the dynamic performance of the pantograph-catenary system, and the feedback linearized LQR control effect is slightly better than the PID

Table 1: Pantograph parameters [16, 23].

Parameters	Type I	Type II
m_1/kg	8	12
m_2/kg	12	13
k_1/N·m	10000	4740
c_1/N·s·m^{-1}	120	70
c_2/N·s·m^{-1}	30	70
k/N·m	100	100
f_0/N	100	100

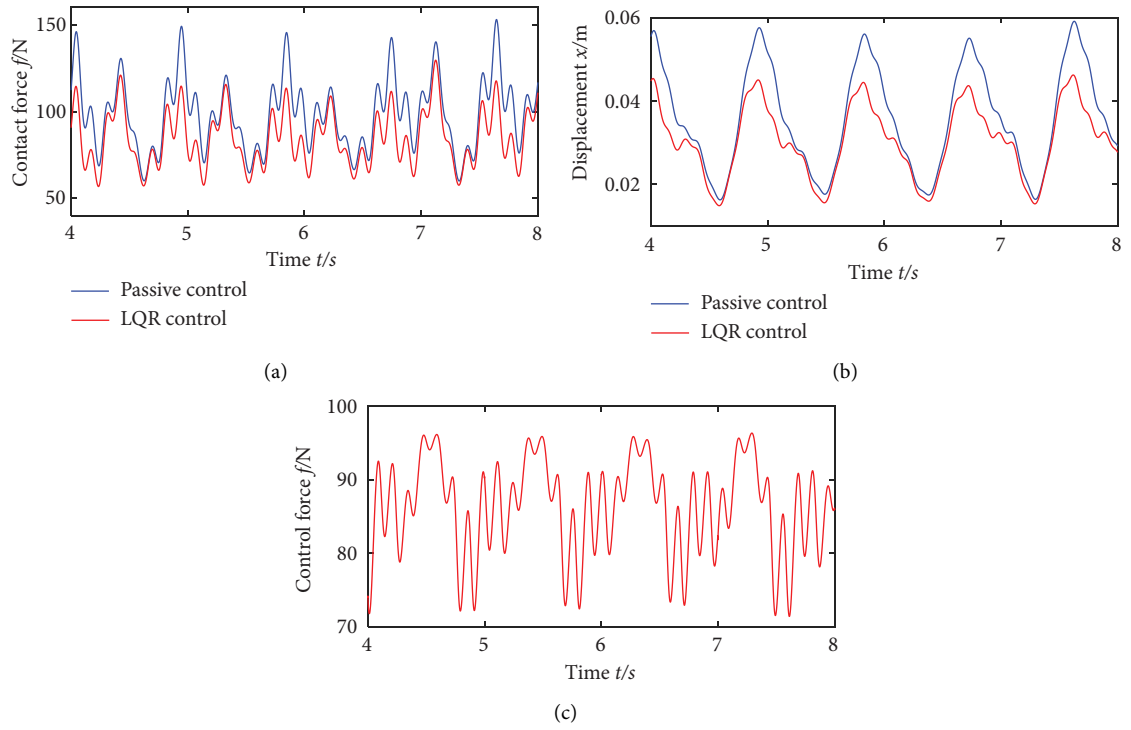

Figure 6: The results of Type I pantograph. (a) Comparison of contact force. (b) Comparison of pantograph head displacement. (c)Active control force response.

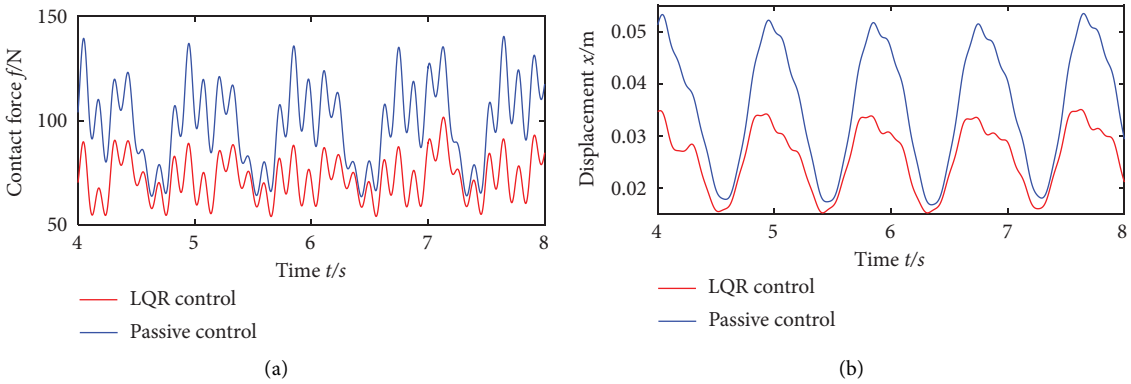

Figure 7: Continued.

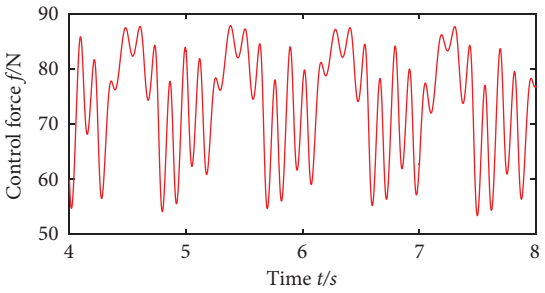

(c)

Figure 7: The results of Type II pantograph. (a) Comparison of contact force. (b) Comparison of pantograph head displacement. (c) Active control force response.

Table 2: Performance index of type I pantograph.

(a) Statistical comparison of pantograph-catenary contact force				
Control modes	Max/N	Min/N	Mean/N	STD
Passive control	167.14	46.20	98.46	20.73
Feedback linearized LQR active control	131.60	42.29	85.11	15.97
(b) Statistical comparison of pantograph head displacement				
Passive control	0.064	0.013	0.036	0.013
Feedback linearized LQR active control	0.051	0.011	0.030	0.009

Table 3: Simulation performance index of type II pantograph parameters.

(a) Statistical comparison of pantograph-catenary contact force.				
Control modes	Max/N	Min/N	Mean/N	STD
Passive control	146.60	45.38	98.25	20.72
Feedback linearized LQR active control	116.27	43.24	72.84	10.67
(b) Statistical comparison of pantograph head displacement				
Passive control	0.060	0.014	0.036	0.012
Feedback linearized LQR active control	0.040	0.013	0.026	0.006

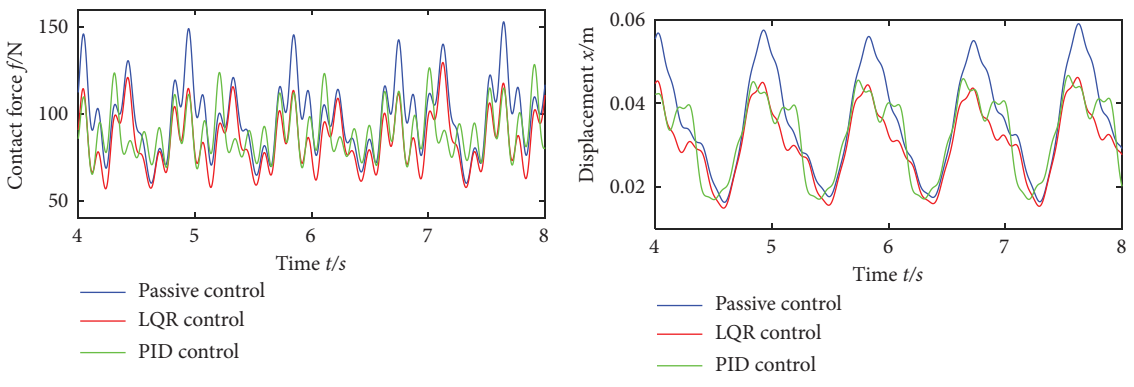

(a) (b)

Figure 8: Continued.

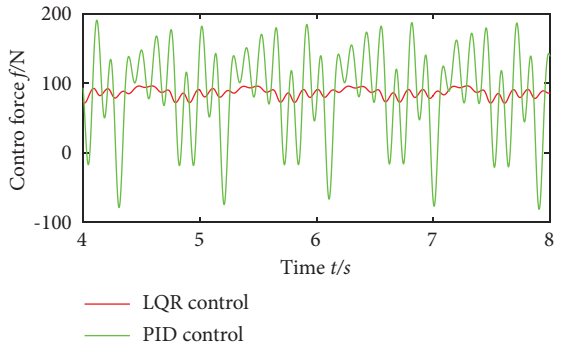

(c)

Figure 8: Comparison of control effects between the two control methods. (a) Comparison of contact force. (b) Comparison of pantograph head displacement. (c) Comparison of active control force.

Table 4: Statistical comparison between the two control methods (v = 250 km/h).

Control modes	Max/N	Min/N	Mean/N	STD
(a) Statistical comparison of pantograph-catenary contact force.				
Passive control	167.14	46.21	98.46	20.74
Feedback linearized LQR active control	131.59	42.29	85.10	15.97
PID control	137.24	63.69	92.40	14.25
(b) Statistical comparison of pantograph head displacement.				
Passive control	0.064	0.013	0.035	0.013
Feedback linearized LQR active control	0.051	0.012	0.030	0.009
PID control	0.051	0.016	0.033	0.010
(c) Statistical comparison of active control force.				
Feedback linearized LQR active control	99.02	66.48	86.49	6.47
PID active control	202.98	-92.92	93.07	64.27

control. Compared with the passive control, the feedback linearized LQR control reduces the mean and the standard deviation of contact force by 14% and 23%, respectively. Compared with the PID control, the active control force fluctuation range of the feedback linearized LQR control is smaller, the mean value is reduced by 8%, and the standard deviation is much smaller than the PID control force. It is shown that, compared with PID control, feedback linearized LQR control can achieve a better control effect with relatively stable and smaller control force, which is beneficial to reduce the energy consumed by the active control of pantograph. At the same time, the smaller fluctuation range can also reduce the adverse effects of time delay.

4.3. Simulation Analysis at Different Train Speeds. In reality, train speed is not a constant value, and it is always changing according to real-time acceleration and deceleration. Therefore, analyzing the response of the pantograph at different train speeds is helpful to better understand the control effect of the control method. Type I pantograph is adopted, and the train speed is increased from 200 km/h to 350 km/h and the step length is 50 km/h. Passive control simulation and feedback linearization LQR control simulation are carried out. The simulation results are shown in Figure 9. Figures 9(a) and 9(b) show the comparison of the maximum, minimum, and average values of contact force and pantograph head displacement at different speeds, respectively. Figure 9(c) shows the maximum, minimum, and average value of the control force for active control. As can be seen from Figure 9, with the increase of train speed, the statistical values of pantograph-catenary contact force and pantograph head displacement under passive control gradually increase, while feedback linearization LQR active control can effectively reduce the pantograph-catenary contact force and pantograph head displacement at different train speeds. At the same time, the average value of the active control force also increases with the increase of speed, and the fluctuation remains within a reasonable range.

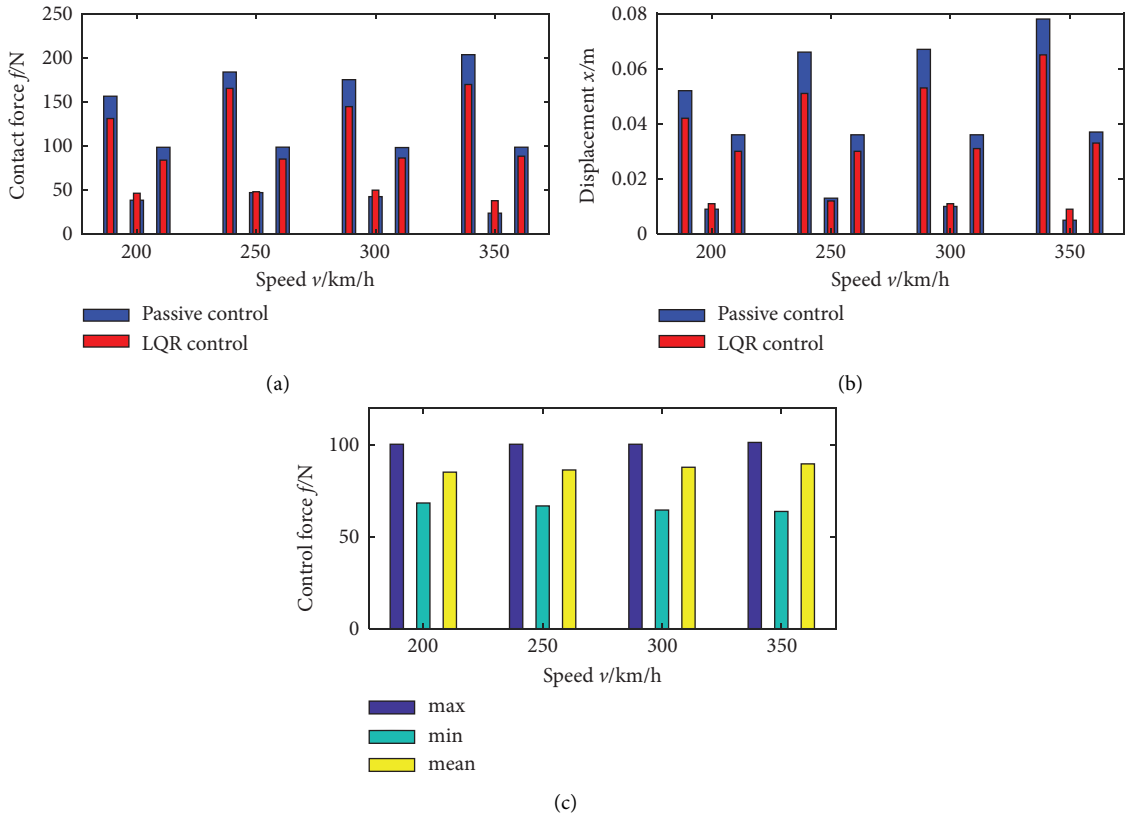

FIGURE 9: Comparison of performance indexes of pantograph-catenary with increasing speed. (a) Contact force statistics. (b) Pantograph head displacement statistics. (c) Active control force statistics.

5. Conclusion

In this paper, considering the influence of fractional-order devices such as air springs between the pantograph and the locomotive body, a two-degree-of-freedom fractional-order pantograph-catenary model is established. Its dynamic equation is given, and the fractional-order differential term is approximated by the Oustaloup filter algorithm. The extended variable method is used to deal with the time-varying stiffness of the catenary, the extended model of pantograph-catenary is linearized by the differential geometry method, and the LQR active controller was designed based on state feedback. Through simulation analysis, the control effect of feedback linearized LQR active control is analyzed and compared with the PID control. Furthermore, the control effect of feedback linearized LQR active control at different train speeds is analyzed. The main conclusions can be drawn as follows: (1) For different types of pantographs, although the feedback linearization LQR active control has different effects, but it can still effectively reduce the vibration amplitude of the pantograph head and the contact force between the pantograph and the catenary. (2) Compared with PID control, feedback linearized LQR active control has a similar effect in decreasing pantograph head vibration amplitude and pantograph-catenary contact force. However, considering the control force size, frequency, and peak value, feedback linearized LQR active control can achieve better control effects with relatively stable control force fluctuations. From the perspective of time delay and energy, it believes that feedback linearized LQR active control is better than PID control. (3) As train speed increases, the time-varying stiffness frequency of the catenary also increases. Feedback linearized LQR active control can play a better control effect at different train speeds.

Data Availability

The data used to support the findings of this study are included within the article.

Conflicts of Interest

The authors declare that they have no conflicts of interest.

Acknowledgments

The authors are grateful to the support by the National Natural Science Foundation of China (12072206, U1934201, 11972237) and the Education Department Project of Hebei Province (ZD2020310).

References

[1] J. H. Lee and T. W. Park, "Development of a three-dimensional catenary model using cable elements based on absolute nodal coordinate formulation," *Journal of Mechanical Science and Technology*, vol. 26, no. 12, pp. 3933–3941, 2012.

[2] J. P. Massat, C. Laurent, J. P. Bianchi, and E. Balmes, "Pantograph catenary dynamic optimisation based on advanced multibody and finite element co-simulation tools," *Vehicle System Dynamics*, vol. 52, no. sup1, pp. 338–354, 2014.

[3] Y. Hu, P. Huang, and R. Ma, "A study on the transient dynamic performance of integral dropper of simple chain suspension catenary," *Journal of Vibration and Shock*, vol. 40, no. 8, pp. 131–136, 2021.

[4] W. Zhang, "Study on dynamics of coupled systems in high-speed trains," *Engineering Sciences*, vol. 17, no. 4, pp. 42–52, 2015.

[5] J. Gil, S. Gregori, M. Tur, and F. J. Fuenmayor, "Analytical model of the pantograph–catenary dynamic interaction and comparison with numerical simulations," *Vehicle System Dynamics*, vol. 60, no. 1, pp. 132–155, 2022.

[6] W. Zhang, D. Zou, M. Tan, N. Zhou, R. Li, and G. Mei, "Review of pantograph and catenary interaction," *Frontiers of Mechanical Engineering*, vol. 13, no. 2, pp. 311–322, 2018.

[7] A. Lopes and J. Machado, "Fractional-order model of a nonlinear inductor," *Bulletin of the Polish Academy of Sciences, Technical Sciences*, vol. 67, no. 1, pp. 61–67, 2019.

[8] X. Liu, H. Li, and Y. Huang, "Fractional derivative bingham model of mr damper," *Journal of Mechanical Electrical Engineering*, vol. 32, no. 3, pp. 338–342, 2015.

[9] Q. Zhang, X. Gu, and J. Ding, "Creep damage model and damage evolution of asphalt mixtures," *Journal of Traffic and Transportation Engineering*, vol. 21, no. 5, pp. 104–113, 2021.

[10] Y. Peng, J. Zhao, and Y. Li, "A wellbore creep model based on the fractional viscoelastic constitutive equation," *Petroleum Exploration and Development*, vol. 44, no. 6, pp. 982–988, 2017.

[11] E. Mark, E. Elbert, and A. Miguel, "Chaotic, fractional, and complex dynamics: new insights and perspectives," *Spring*, vol. 24, p. 56, 2017.

[12] D. Xue, *Fractional-Order Control Systems: Fundamentals and Numerical Implementations[M]*, De Gruyter, Berlin, Boston, 2017.

[13] J. Guo, S. Yang, and G. Gao, "Research on active control of the pantograph-catenary system with varying stiffness," *Journal of Vibration and Shock*, no. 2, pp. 15–144, 2005.

[14] Z. Chen, B. Tang, and G. Shi, "Design of the pantograph optimal tracking controller based on linear Quadratic," *Journal of Electronic Measurement and Instrument*, vol. 29, no. 11, pp. 1647–1654, 2015.

[15] G. Shi, Z. Chen, and F. Guo, "Feedback linearization control of load between pantograph and catenary," *Control Theory & Applications*, vol. 33, no. 1, pp. 85–91, 2016, (in Chinese).

[16] K.-K. Zhang, Z. Mao, and B. Jiang, "Adaptive and robust fault-tolerant tracking control of contact force of pantograph-catenary for high-speed trains," *IFAC-PapersOnLine*, vol. 48, no. 21, pp. 740–745, 2015.

[17] B. Zhu, Z. Ren, and W. Xie, "Active nonlinear partial-state feedback control of contacting force for a pantograph–catenary system," *ISA Transactions*, vol. 91, pp. 78–89, 2019.

[18] Y. Song and L. Li, "Robust adaptive contact force control of pantograph–catenary system: an accelerated output feedback approach," *IEEE Transactions on Industrial Electronics*, vol. 68, no. 8, pp. 7391–7399, 2021.

[19] Z. Zhuang, Y. Shi, and X. Chen, "Globally active feedback-linearization control strategy for pantograph-catenary system," in *Proceedings of 2016 3rd International Conference on Information and Communication Technology for Education (ICTE 2016)*, pp. 335–341, 2016.

[20] P. Alessandro and U. Elio, "Contact force regulation in wire-actuated pantographs via variable structure control and frequency-domain techniques," *International Journal of Control*, vol. 81, no. 11, p. 352, 2008.

[21] A. Pisano and E. Usai, "Contact force estimation and regulation in active pantographs: an algebraic observability approach," *Asian Journal of Control*, vol. 13, no. 6, pp. 761–772, 2011.

[22] A. Pisano and E. Usai, "Contact force regulation in wire-actuated pantographs via variable structure control and frequency-domain techniques," *International Journal of Control*, vol. 81, no. 11, pp. 1747–1762, 2008.

[23] M. A. Karkoub and M. Zribi, "Active/semi-active suspension control using magnetorheological actuators," *International Journal of Systems Science*, vol. 37, no. 1, pp. 35–44, 2006.

[24] R. Chen, S. Wang, and L. Yang, "Active control and simulation for pantograph based on contact force prediction of long short-term memory network," *Chinese Journal of Scientific Instrument*, vol. 42, no. 05, pp. 192–198, 2021.

[25] A. Mosavi, M. Shokri, Z. Mansor, S. N. Qasem, S. S. Band, and A. Mohammadzadeh, "Machine learning for modeling the singular multi-pantograph equations," *Entropy*, vol. 22, no. 9, p. 1041, 2020.

[26] T. C. Lin, C. W. Sun, Y. C. Lin, and M. M. Zirkohi, "Intelligent contact force regulation of pantograph–catenary based on novel type-reduction technology," *Electronics*, vol. 11, no. 1, p. 132, 2022.

[27] E. Karakose, M. T. Gencoglu, M. Karakose, O. Yaman, I. Aydin, and E. Akin, "A new arc detection method based on fuzzy logic using S-transform for pantograph–catenary systems," *Journal of Intelligent Manufacturing*, vol. 29, no. 4, pp. 839–856, 2018.

[28] Z. Paweł, A. Adam M, and T. Uhl, "An investigation on the active control strategy for a high-speed pantograph using co-simulations," *Journal of Systems and Control Engineering*, vol. 233, no. 4, pp. 370–383, 2019.

[29] H. Ren, H. Zhang, G. Deng, and B. Hou, "Feedforward feedback pitch control for wind turbine based on feedback linearization with sliding mode and fuzzy PID algorithm," *Mathematical Problems in Engineering*, vol. 24, pp. 270–289, 2018.

[30] L. Zheng, Y. Zhao, and S. Chen, "A dual-observer design for nonlinear suspension system based on feedback linearization," *Mathematical Problems in Engineering*, vol. 388, p. 2353, 2018.

[31] Z. Xia, "Design of static output feedback controller for fractional-order T-S fuzzy system," *Mathematical Problems in Engineering*, p. 2997, 2020.

[32] Z. Qi, X. Wang, and R. Mo, "Air spring modeling and vehicle dynamics analysis based on fractional calculus theory," *Journal of the China Railway Society*, vol. 43, no. 04, pp. 67–76, 2021.

[33] A. Alkamachi and E. Erçelebi, "H_∞ control of an overactuated tilt rotors quadcopter," *Journal of Central South University*, vol. 25, no. 3, pp. 586–599, 2018.

[34] J. E. Slotine and W. Li, *Applied Nonlinear Control*, Prentice-Hall, New Jersey, 1991.